

An Information Driven Approach For Ego-Lane Detection Using Lidar And OpenStreetMap

Abderrahim KASMI^{1,2}, Johann LACONTE², Romuald AUFRERE², Ruddy THEODOSE^{1,2}, Dieumet DENIS¹, Roland CHAPUIS²

Abstract—Localizing the vehicle in its lane is a critical task for any autonomous vehicle. By and large, this task is carried out primarily through the identification of ego-lane markings. In recent years, ego-lane marking detection systems have been the subject of various research topics, using several inputs data such as camera or lidar sensors. Lately, the current trend is to use high accurate maps (HD maps) that provide accurate information about the road environment. However, these maps suffer from their availability and their price tag. An alternative is the use of affordable low-accurate maps. Yet, there is relatively little work on it. In this paper, we propose an information-driven approach that takes into account inaccurate prior geometry of the road from OpenStreetMap (OSM) to perform ego-lane marking detection using solely a lidar. The two major novelties presented in this paper are the use of the OSM datasets as prior for the road geometry, which reduces the research area in the lidar space, and the information-driven approach, which guarantees that the outcome of the detection is coherent to the road geometry. The robustness of the proposed method is proven on real datasets and statistical metrics are used to highlight our method’s efficiency.

I. INTRODUCTION

Accurate self-vehicle localization is an important task for autonomous driving and advanced driver-assistance systems (ADAS). Indeed, for some ADAS applications like Lane Keeping Assist, knowing the position of a vehicle within the host lane in the road is crucial in ensuring adequate maneuvering instructions and vehicle safety.

Several localization strategies have sprung up to fit the lane/road understanding requirements entirely. One of the most well-known techniques incorporates an inertial measurement unit (IMU) with a classic global navigation satellite system (GNSS) receiver (e.g., GPS, Galileo) to locate the ego-vehicle. However, according to the GPS performance analysis report of the Federal Aviation Administration [1], the accuracy of a standard GNSS receiver device is within 3 m with a 95% confidence that does not meet the requirements needed for most ADAS applications.

One solution for having an accurate localization that satisfies the criteria is to locate the vehicle with respect to certain visual landmarks. Lane markings are the most used in that

context since they are the easiest to identify and provide more detail about the road. Leafing through the literature, it appears that most researchers use a camera for lane marking detection [2]. Indeed, there are two main advantages of using the camera: currently, this sensor is the cheapest and most reliable modality for automotive applications and it provides dense information of the environment. However, this sensor depends on the lightness conditions which entails a filtering process. To overcome this issue lidar sensors can be used. Using lidar data, it is possible to determine whether a lidar beam has intercepted asphalt or road painting regardless of the lighting conditions [3]. This specifically helps in coping with shadows and darkness where cameras struggle. Besides, lidar offers a centimeter-accurate 3D representation of the world. In counterpart, lidar is more expensive than cameras. Nevertheless, the progress in optical technology and the increasing demand ultimately led to a decline in the price of the lidar.

Detection of lane markings using lidar has been the topic of several research works. Starting with the 2007 DARPA Urban Challenge, the authors in [4] presented a road edge (curb) detection using a 2D lidar. In [5] authors proposed a method to detect road marking. The method relies on an Otsu thresholding that allows the separation between asphalt and road marking. Lately, Convolutional Neural Networks (CNN) have been spread out for ego-lane detection for images [6]. Before computing the convolutions, a process phase is included that transforms the lidar points cloud into reflectivity images, then the generated images are fed into a neural network [7]. Authors in [8] presented a data-driven approach for ego-lane marking recognition based on several 3D lidars. A mask is designed using the position of the vehicle in order to extract ego-lane marking. However, a problem arises when the algorithm miss matched the ego-lane marking. Indeed, the outcome produced is incoherent with the geometry of the lane marking. In contrast, this work presents a probabilistic model that guarantees the coherence between the right and left ego lane marking, which results in a coherent geometry for the ego-lane marking.

High Definition (HD) maps have also been coupled with lidar in order to provide accurate localization. In [9], the authors used a lane-level localization based on lidar sensor to match with an HD map. Lane markings are implemented in two different steps: road segmentation and Hough Transform on an intensity image, the resulting lanes are matched with an HD map to enhance the vehicle localization. According

*This work has been sponsored by Sherpa Engineering and ANRT (Conventions Industrielles de Formation par la Recherche).

¹ Sherpa Engineering, R&D Department, 333 Avenue Georges Clemenceau, 92000 Nanterre, France. [a.kasmi, d.denis]@sherpa-eng.com

² Université Clermont Auvergne, CNRS, SIGMA Clermont, Institut Pascal, F-63000 Clermont-Ferrand, France. FirstName.LastName@uca.fr

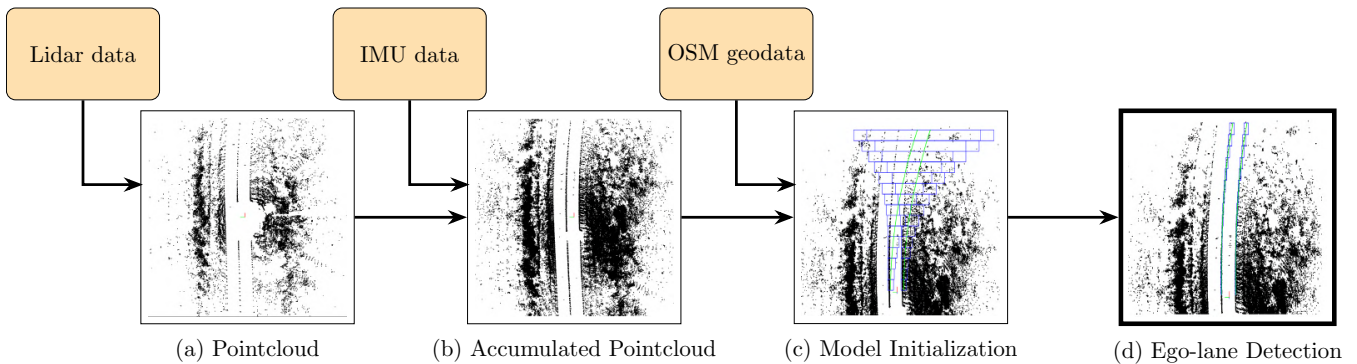


Fig. 1: Overall algorithm for the proposed ego-lane detection. (a) The lidar provides pointclouds. (b) Using an IMU, several pointclouds are accumulated. (c) The ego-lane detection is initialized with OSM geodata. In blue, the search area corresponding to the uncertainty zone with its mean value in green. (d) the final ego-lane marking detection results after convergence.

to [8], there are two main drawbacks of HD maps: the first one is the cost involving creating them. The second one is the availability for all the geographical locations. Indeed, creating an HD map of the entire road structure of the world is impossible due to the constant evolution of the roads. These two drawbacks make high definition (HD) maps as an intelligent sensor incapable of replacing the already existing solutions (cameras and lidars). Furthermore, as human beings, we do not need such a high precision map to be conscious of where the road is. Therefore, in this work, we present a method closer to the human process where we only have a coarse approximation of the road map.

A more affordable alternative to HD maps is the collaborative maps like OpenStreetMap (OSM). In the field of intelligent transport system, OSM data-sets have been used for several tasks like Road-level localization [10], Lane-level determination [11]. An interesting approach is presented in [12]. It relies on the use of road priors and contextual information for road detection using camera images. Depending on the number of lanes and the width of the lane, OSM map is used to build the road backbone. This road shape is then projected onto the image taking into account the uncertainties related to the ego-vehicle pose. The result is used as prior to roadway detection. Worth mentioning study presented in [13] uses OSM data prior to generating a more accurate map. Indeed, the authors present a fusion framework from the OSM data and proprioceptive sensors. In this paper, we use a similar process as we benefit from the road geometry information extracted from OSM to detect the ego-lane marking in the lidar pointclouds. To the best of our knowledge, no study has been conducted to use a low-cost map such as OSM with lidar data.

In this paper, it is proposed an ego-lane marking detection framework that uses only a single lidar and an OSM map. There are two main novelties presented in this work are

- the use of a coarse map (OSM) to have *a priori* about road geometry; and
- the information-driven approach used in the recognition step. We adopt the information entropy features in order

to increase the signal to noise ratio in the recognition procedure and ultimately reduce the computation complexity. Furthermore, the probabilistic model proposed will ensure the geometric coherency between ego-lane marking.

II. OVERALL ALGORITHM

The pipeline of the proposed ego-lane marking algorithm is illustrated in Figure 1. The method is divided into three steps: Firstly, the raw point cloud is processed by taking into account the five last frames. This process is performed using the vehicle state information from an IMU (Inertial Measurement Unit). Thereupon, the road model is extracted from OSM and this model is projected into the lidar reference. Finally, using this probabilistic model as prior, recursive recognition detection is performed. All steps of this algorithm are described in detail in the following sections.

A. Lidar point cloud process

The lidar frames are rich in information. However, one single lidar frame is not sufficiently dense to correctly perform the ego-lane recognition. To overcome this drawback, we integrate the previous lidar frames into one frame based on the odometry information of the vehicle. For this work, we took the last 5 frames into account. Figure 1(a) and Figure 1(b) show the difference in the sparseness of the lidar pointclouds.

We apply then a threshold on reflectivity. Since we are looking for the ego-lane marking, points cloud with high reflectivity will be chosen.

B. Initialization of 2D model: OSM dataset

Before starting with this stage, we must briefly present the OSM data. Basically, the OSM data are composed of three keys components: Nodes, Ways, and Relations [14]. Nodes are the geometrical elements that represent GPS points. Ways are an ordered list of nodes that represents the roads network. Thus, each Way (road) is composed of a set of segments [10]. In other words, belonging to a segment is equivalent to belonging to an OSM Way. So the map matching task can

be reformulated as matching a GPS point with a segment. Therefore, we use the map-matching algorithm presented in [10] in order to choose the correct Way (road).

Once the road has been selected, the road is modeled in 2D lidar frame (x, y) as a cubic polynomial as shown on Figure 2 with x in the forward direction and y in the left direction [15]:

$$y(x) = \frac{1}{6} c' x^3 + \frac{1}{2} c_0 x^2 + \psi x + d_0 \quad (1)$$

The parameters c' is the curvature's derivative of the road, c_0 the curvature of the road, ψ the vehicle's heading with respect of the tangent of the road, d_0 the lateral shift of the ego-vehicle in relation to the road model. For a lane of width L_w , the left and right ego-lane markings are

$$y_{l,r}(x) = y(x) \pm \frac{1}{2} \frac{L_w}{\sqrt{1 + y'(x)^2}}, \quad (2)$$

where $y'(x) = \frac{d}{dx}y(x)$. One can note that the equation for the markings is not polynomial. However, as the curvature of the road is small on the highways and most marked roads, the derivative $y'(x)$ can be neglected for small x . The equation simplifies to

$$y_{l,r}(x) \approx y(x) \pm \frac{1}{2} L_w. \quad (3)$$

In practice, the approximation even holds for large x , being accurate enough up to 50 m.

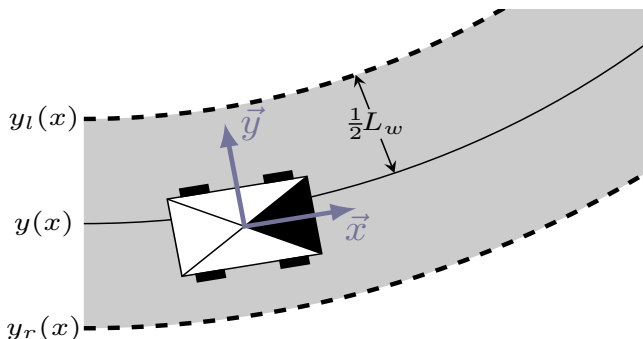


Fig. 2: The robot navigates on the lane of width L_w modeled as a polynomial equation $y(x)$. The left and right borders of the lane are respectively approximated with the polynomials $y_l(x)$ and $y_r(x)$.

As discussed before, the OSM data lacks information about precision. As a consequence, the coefficients of the cubic polynomial defined in Equation 3 are not accurate. However, the two coefficients c' and c_0 represent the global shape of the road so their values can be used as an estimation.

To encompass these uncertainties for each ego-lane marking, we define a probabilistic model composed of a state vector $s_{l,r}$ and its associated covariance matrix $C_{s_{l,r}}$. The state vector $s_{l,r}$ is defined as

$$s_{l,r} = [\mu_{c'}, \mu_{c_0}, \mu_{\psi}, \mu_{d_0}, \mu_{L_w}]^T, \quad (4)$$

with μ refereeing to a mean value. The values $(\mu_{c'}, \mu_{c_0})$ are taken from OSM (Equation 1). These values are not

necessarily accurate but will be counterbalanced by taking into account the incertitude on the vector $s_{l,r}$. The covariance matrix $C_{s_{l,r}}$ is initialized as

$$C_{s_{l,r}} = \begin{pmatrix} \sigma_{c'}^2 & 0 & 0 & 0 & 0 \\ 0 & \sigma_{c_0}^2 & 0 & 0 & 0 \\ 0 & 0 & \sigma_{\psi}^2 & 0 & 0 \\ 0 & 0 & 0 & \sigma_{d_0}^2 & 0 \\ 0 & 0 & 0 & 0 & \sigma_{L_w}^2 \end{pmatrix}. \quad (5)$$

We project this model on the lidar frame in order to get the uncertainty about the cubic polynomial. To do so we compute the Jacobian matrix of the polynomials $y_{l,r}(x)$:

$$J_{y_{l,r}} = \begin{pmatrix} \frac{\partial y_{l,r}}{\partial c'} & \frac{\partial y_{l,r}}{\partial c_0} & \frac{\partial y_{l,r}}{\partial \psi} & \frac{\partial y_{l,r}}{\partial d_0} & \frac{\partial y_{l,r}}{\partial L_w} \end{pmatrix} \quad (6)$$

Thus, we have:

$$C_{y_{l,r}} = J_{y_{l,r}} C_{s_{l,r}} J_{y_{l,r}}^T. \quad (7)$$

The resulting model $(y_{l,r}, C_{y_{l,r}})$ is transformed into the lidar space as illustrated in Figure 3 with $C_{y_{l,r}}$ representing the uncertainties and thus defining the search area for the ego-lane marking.

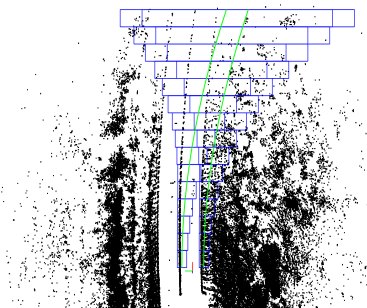


Fig. 3: Intensity image of the lidar points with the model initialization of the presented ego-lane marking model. The green line is used for the mean value of the probabilistic model represented by the vectors $y_{l,r}$, and the blue rectangles are used to represent the uncertainty $C_{y_{l,r}}$.

C. Recursive entropic recognition

Once the probabilistic model is defined, we proceed to the recognition phase. In contrast to what is described in most of the works available for lidar detection, we present an informational driven approach that is inspired by the work of [16] for camera images. The concept is based on a focusing algorithm to detect the ego-lane marking. To do so, we take advantage of the initialized probabilistic model $(y_{l,r}, C_{y_{l,r}})$ in order to limit the search areas for the ego-lane marking. Once the search area created, we divide this zone into n_{roi} Regions Of Interest (ROI) that has the same height. Afterward, we developed a Bayesian Network (BN) coupled with the entropic features to choose the most informative ROI, which means the ROI where we have the best chance of detecting a section (a segment) of the ego lane marking. After each detection, we update the probabilistic model $(y_{l,r}, C_{y_{l,r}})$ which leads to a new searching area and

accordingly reduce the size of the ROIs.

One of the main advantages of this method appears in the case of wrong detection of a segment. This wrong detection will produce a wrong probabilistic model. Hence the resulting ROIs will no longer cover the ego-lane marking. If this scenario happens, the recursive nature of the proposed method allows us to downgrade to the previous probabilistic methods. These steps are repeated until an entropic criterion is achieved indicating that the ego-lane marking has been detected. The overall architecture of the discussed algorithm is presented in Figure 4. Each part of the algorithm is detailed in the following:

- i **Initialization** At this stage we define the initial probabilistic model $(\mathbf{y}_{l,r}, \mathbf{C}_{\mathbf{y}_{l,r}})$ as already presented in Section II-B.
- ii **Selection of the best Region Of Interest (ROI)** Once the probabilistic model is defined, we proceed to the selection of the most informative ROI in a **Top-Down process** fashion. To do so, we use Entropy from Shannon's information [17], because it measures the uncertainty about a random variable. To select the most informative ROI we use an *a priori* selection, we compute the entropy improvement between the ego-lane state before attempting a detection and after simulating a detection. Thus, we define the informational criterion H_{sel} :

$$\begin{aligned} H_{sel} &\triangleq \Delta H \\ &= H_e^- - H_e^+ \end{aligned} \quad (8)$$

With H_e^- the entropy of the ego-lane state before detection and H_e^+ the entropy of the ego-lane state after detection. Thus, H_e^+ depends on the simulated detection result. As results H_{sel} is computed as

$$\begin{aligned} H_{sel} &= H_e^- - H_e^+ \\ &= p(D_k = 1, D_b = 1) \cdot \frac{1}{2} \left[\log|2\pi e C_{\mathbf{y}_{l,r}}^-| - \log|2\pi e C_{\mathbf{y}_{l,r}}^+| \right], \end{aligned} \quad (9)$$

with:

$$\begin{cases} \mathbf{C}_{\mathbf{y}_{l,r}}^- & \text{Covariance before simulation of the detection, and} \\ \mathbf{C}_{\mathbf{y}_{l,r}}^+ & \text{Covariance after simulation of the detection.} \end{cases}$$

For the probabilities, $p(D_b), p(D_k)$, a Bayesian Network is introduced [18]. Bayesian networks are generally used to formalize knowledge in an uncertain environment and are therefore entirely appropriate in this case [19]. The scheme of our Bayesian network is illustrated in Figure 5. Events modeled in the BN are the following:

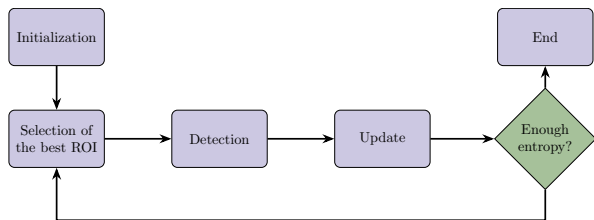


Fig. 4: All different steps of the Recognition stage for ego-lane marking detection.

- X_{k-} , the confidence before the detection is attempted
- Z_0 , the chosen landmark (the white strip) is observable in the ROI
- D_k , a landmark is detected in the focal zone,
- D_b , the correct landmark has been detected (which manages landmark ambiguity)
- X_{k+} , the confidence after the detection is attempted (success or failure)

This BN can take into account several uncertainties: the detector's performances in the node D_k , the Observability of the segment in the ROI modeled in the node Z_0 and the ambiguity in the node D_b . Also, this network has two main uses, the first one is to calculate the *a priori* probabilities $p(D_k)$ and $p(D_b)$ for the entropic criterion H_{sel} and the second one is to determine the confidence $p(X_{k+})$ obtained after proceeding to a detection.

- iii **Detection** Once the most informative ROI is chosen, we proceed to the detection. The idea is based on a RANSAC method, which is used in order to detect the segment in the ROI. Thus, for each ROI two points $p_1(x_1, y_1)$ and $p_2(x_2, y_2)$ are defined.
- iv **Update** For the state vector $y_p = (y_1, y_2)$ we associate a co-variance matrix \mathbf{C}_{y_p} :

$$\mathbf{C}_{y_p} = \begin{pmatrix} \sigma_{y_t}^2 & 0 \\ 0 & \sigma_{y_b}^2 \end{pmatrix} \quad (10)$$

With $(\sigma_{y_t}^2, \sigma_{y_b}^2)$ being the accuracy of the segment detected. In order to update the probabilistic model, we use a Kalman filter:

$$\begin{cases} \mathbf{y}_{l,r}^+ = \mathbf{y}_{l,r}^- + K [\hat{y}_p - y_p] \\ \mathbf{C}_{\mathbf{y}_{l,r}}^+ = \mathbf{C}_{\mathbf{y}_{l,r}}^- - KH_c \mathbf{C}_{\mathbf{y}_{l,r}}^- \end{cases} \quad (11)$$

with K being the Kalman Gain, $(\mathbf{y}_{l,r}^-, \mathbf{C}_{\mathbf{y}_{l,r}}^-)$ is the model before detection, $(\mathbf{y}_{l,r}^+, \mathbf{C}_{\mathbf{y}_{l,r}}^+)$ is the model after detection and H_c the matrix linking \mathbf{C}_{y_p} to $\mathbf{C}_{\mathbf{y}_{l,r}}^+$.

- v **End** After each detection, we want to know if the ego-lane detection recognition is completed. This operation is performed using the entropy as presented in Item ii. To this end, we define an entropic criterion H_{gain} that will compute the entropy improvement between the initial covariance state $\mathbf{C}_{\mathbf{y}_{l,r}}^*$ and the current covariance state $\mathbf{C}_{\mathbf{y}_{l,r}}$. In addition, this criterion takes into account the

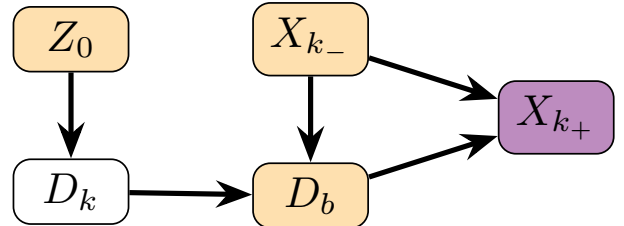


Fig. 5: Bayesian Network used for the confidence estimation. Yellow nodes are the input nodes, Purple nodes are the output nodes, and White is for the observable nodes.

confidence in the current state expressed by the probability $p(X_k^+)$. Thus H_{gain} is computed as

$$H_{gain} = p(X_k^+) \cdot \frac{1}{2} \left[\log|2\pi e \mathbf{C}_{y_{l,r}}^*| - \log|2\pi e \mathbf{C}_{y_{l,r}}| \right]. \quad (12)$$

The ego-lane marking has been detected if the following condition is satisfied:

$$H_{gain} \geq \lambda H_{max} \quad (13)$$

with H_{max} the entropy improvement if the detections were successful in all the ROIs and $\lambda \in [0, 1]$. If the condition is satisfied, it means that enough detections have been attempted successfully and the probabilistic model $(\mathbf{y}_{l,r}^+, \mathbf{C}_{y_{l,r}}^+)$ obtained is sufficiently precise to consider the ego-lane recognition finished. Otherwise, the ego-lane recognition process is carried out, and the second most informative ROI is selected.

In the end of this process, an estimation of the model $(\mathbf{y}_{l,r}^+, \mathbf{C}_{y_{l,r}}^+)$ is obtained.

D. Tracking step

The main objective of this module is to provide a smaller confidence interval for the frame $k+1$ than the one provided by the initial probabilistic model, which means smaller values for matrix $\mathbf{C}_{y_{l,r}}$. Thus, we have to compute $\mathbf{y}_{l,r}(k+1)$ and $\mathbf{C}_{y_{l,r}}(k+1)$ from $\mathbf{y}_{l,r}(k)$ and $\mathbf{C}_{y_{l,r}}(k)$ and the odometry information from the vehicle. To do so, we define a general vector $\mathbf{y} = (\mathbf{s}_{l,r}, \mathbf{y}_{l,r})$ which contains the 2D vector $\mathbf{s}_{l,r}$ and the polynomial vector $\mathbf{y}_{l,r}$ and \mathbf{C}_y its covariance matrix. The initial value of $(\mathbf{y}(0), \mathbf{C}_y(0))$ can be easily computed using the same strategy presented in Section II-B. Thus, we start computing the evolution of the model $(\mathbf{s}_{l,r}, \mathbf{C}_{s_{l,r}})$ as follows:

$$\begin{cases} \mathbf{s}_{l,r}(k+1) = \mathbf{M} \mathbf{s}_{l,r}(k) + \mathbf{W}_t \\ \mathbf{C}_{s_{l,r}}(k+1) = \mathbf{M} \mathbf{C}_{s_{l,r}}(k) \mathbf{M}^T + \mathbf{Q} \end{cases} \quad (14)$$

With \mathbf{M} the evolution matrix that includes the displacement and the angle difference for a small time interval. The matrix \mathbf{Q} represents the error in the evolution matrix. Thereafter, we update the new model $(\mathbf{y}(k+1), \mathbf{C}_y(k+1))$ using the model $(\mathbf{y}_{l,r}(k), \mathbf{C}_{y_{l,r}}(k))$ that we get from the recognition step:

$$\begin{cases} \mathbf{y}(k+1) = \mathbf{y}(0) + \mathbf{K}_t [\mathbf{s}_{l,r}(k+1) - \mathbf{s}_{l,r}(0)] \\ \mathbf{C}_y(k+1) = \mathbf{C}_y(0) - \mathbf{K}_t \mathbf{H}_t \mathbf{C}_y(k) \end{cases} \quad (15)$$

with $\mathbf{K}_t = \mathbf{C}_y(0) \mathbf{H}_t^T [\mathbf{H}_t \mathbf{C}_y(0) \mathbf{H}_t^T + \mathbf{C}_{s_{l,r}}(k+1)]^{-1}$ and $\mathbf{s}_{l,r} = \mathbf{H}_t \mathbf{y}$. After this update, the vector $\mathbf{y}_{l,r}(k+1)$ and its covariance matrix $\mathbf{C}_{y_{l,r}}(k+1)$, contained in the model $(\mathbf{y}(k+1), \mathbf{C}_y(k+1))$, define a new confidence interval for the next frame.

III. EXPERIMENTAL RESULTS

A. Datasets and metric used for experimental results

In order to show the effectiveness of our lidar-based lane detection system, we investigate on the available datasets for autonomous vehicles. We focus our attention on the datasets

suitable for lane marking detection in highway scenarios.

Taking into account these consideration, it appears that most of the available datasets are not suitable to qualify the effectiveness of our algorithm, mainly for two reasons. The first one, is that most of the datasets do not provide lidar data. The second one is the type of annotation for the Ground Truth. As highlighted by [20], there does not appear to be a consensus among the autonomous driving community on the type of annotation for ego-lane marking. In reality, most datasets use pixel-wise annotation (e.g, KITTI [21], Ego-Lane Analysis System (ELAS) [22], Unsupervised Llamas [23]). This pixel-level annotation is not suitable for us. Indeed, we have a higher level representation of the lane, as we represents the ego-lane marking as polynomial. Of course, someone may point out the Carina datasets [5]. However, to authors knowledge these datasets are still not available.

The absence of suitable GT to analyze the effectiveness of our lidar-based lane detection system brought us to build our own annotation using the KITTI datasets [21]. In order to build our own GT, we first manually annotated the lidar points to determine the ego-lane. For each pointcloud, we transform the pointcloud into Bird's Eye View image. The image has a dimension of 240×600 pixels with each pixel has a size of 0.05×0.05 m. This procedure is repeated for all the sequences. Once the BEV images available, we annotate the ground truth for the ego-lane as illustrated on Figure 6. For the detection performances, several metrics are used in the literature [8]. However, some of these metrics are not suitable for our algorithm, as we have a higher representation of the ego-lane marking (polynomial), we need a metric that unable us to distinguish between an error of 1 cm and one of 1 m. For that reason, we use Root mean squared error (RMSE), it has the benefit of penalizing large errors.

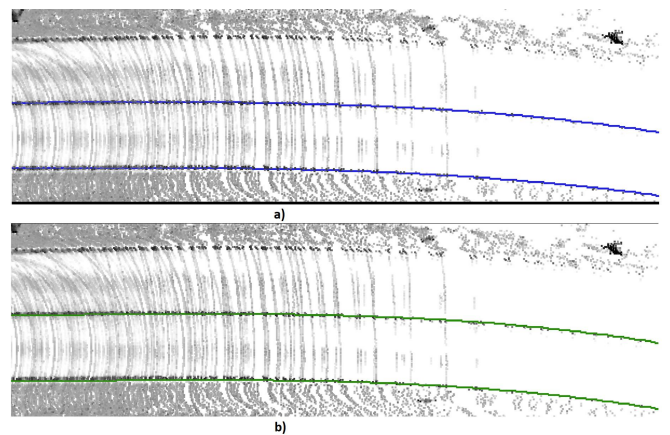


Fig. 6: Process for the evaluation of the detection lane, first a BEV (Bird's Eye View) image is produced with its associated ground truth in blue (a), the result of the detection is transposed in the BEV image in green (b).

B. Experimental results

The parameters used for our experimental are shown in Table I. Authors would like to emphasize that these param-

variable	definition	value
n_{roi}	number of ROIs	20
μ_{d_0}	mean value for distance to center line	0 m
μ_{psi}	mean value for ψ	0 rad
μ_{L_w}	mean value for lane width	3.5 m
$\sigma_{c'}$	standard deviation for the curvature's derivative	10^{-5} m
σ_{c_0}	standard deviation for the curvature	10^{-4} m
σ_{d_0}	standard deviation for distance to center line	0.25 m
σ_{psi}	standard deviation for ψ	0.1 rad
σ_{L_w}	standard deviation for lane width	0.5 m

TABLE I: Parameters used for our experiments

eters were set by hand and no extensive hand tuning was performed. In addition, these parameters are means values that are suitable for highway scenarios. These results are performed on two highway sequences from the KITTI datasets noted as "2011_09_26/0027" and "2011_09_26/0028". The corresponding results for the RMSE are summarized in Figure 7. The average values for the whole sequences are presented in Table II.

The results presented testify about the effectiveness of our proposed algorithm. Accordingly, by taking into account the RMSE in the Figure 7, we found that more than 97.80% of the time the detection error is bellow 0.15 m for sequence 27 and 80.61% for sequence 28. Nevertheless, in the worst cases, the maximum values in Table II are 0.40 m and 0.48 m which shows that even when incorrect detections happen, the error is still acceptable. In addition, when these incorrect detections occur, the outcome result is still coherent as shown on Figure 8. By investigating these cases we found that these scenarios happen when the density of the lidar is not enough sufficient for a good ego-lane marking.

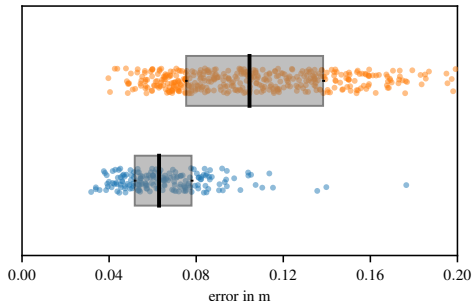


Fig. 7: RMSE of the sequence 27 (a) and of the sequence 28 (b). The color code used is the follow: Orange stands for sequence 27 and Blue for sequence 28

Some qualitative results concerning ego-lane detection are presented in Figure 8. For a visual comparison, the ego-lane

Metrics	Sequence 27	Sequence 28
RMSE (mean)	0.07 m	0.11 m
RMSE (median)	0.06 m	0.10 m
RMSE (max)	0.40 m	0.48 m

TABLE II: Results of RMSE for our experiments on the KITTI dataset.

marking detected were projected on the image and a camera-based detection solution was added.

C. Discussion

The presented results show that the proposed Lidar-based solution is suitable to detect the ego-lane marking. In Figure 8(b) an illustration of a case where the high brightness make the detection of the ego-lane marking difficult for the camera. However, it is not the case when using the ego-lane marking algorithm with the lidar data. However, the most remarkable attribute of the proposed algorithm appears when a miss-match happens, as illustrated in Figure 8(d). Indeed, the outcome is still coherent, the geometry of the lane is preserved. This feature is due to the probabilistic model $(y_{l,r}, C_{y_{l,r}})$, as we take into consideration the shape of road from OSM as prior, the outcome of the detection, even if a miss-match happens, is still coherent, which is not the case when using classic data-driven approach. In [8] when miss-matches occur, it results in a cross-shaped lane marking that is not coherent to the shape of a road, ultimately this kind of method can not be solely used for an autonomous vehicle application. Besides our solution shows good results when detecting the ego-lane marking, it guaranties that even if the detecting process goes wrong, the outcome will be still coherent and acceptable.

IV. CONCLUSION

In this work, we presented an ego-lane marking solution based on lidar data and OpenStreetMap (OSM). It uses an information-driven approach that takes into account inaccurate priors on road's geometry from OpenStreetMap. To do so, a probabilistic model was introduced in order to restricts the region of interests in the lidar domain, Moreover, this probabilistic model ensures the coherence of the results of the ego-lane detection, since it takes into account the geometry restriction of the lane. Unlike other works, our presented framework is differentiated by the use of the OSM data as prior to reduce the space complexity of the detection problem. It also guaranties the coherence of the detected ego-lane marking, as the shape of the detected ego-lane marking is coherent even if miss matches occurs. To conclude, we show that starting from a coarse map, our pure lidar solution reached significant results in term accuracy and consistency. In future work, we aim at coupling this algorithm with a camera-based solution to enhance the proposed framework. Furthermore, we are still working on how to make the most of the OSM data-set as we strongly believe that this kind of map can be an alternative to HD maps.

V. ACKNOWLEDGMENT

This work has been sponsored by Sherpa Engineering and ANRT (Conventions Industrielles de Formation par la Recherche). This work has been sponsored also by the French government research program Investissements d'avenir through the RobotEx Equipment of Excellence (ANR-10-EQPX-44) and the IMobS3 Laboratory of Excellence (ANR-10-LABX-16-01), by the European Union

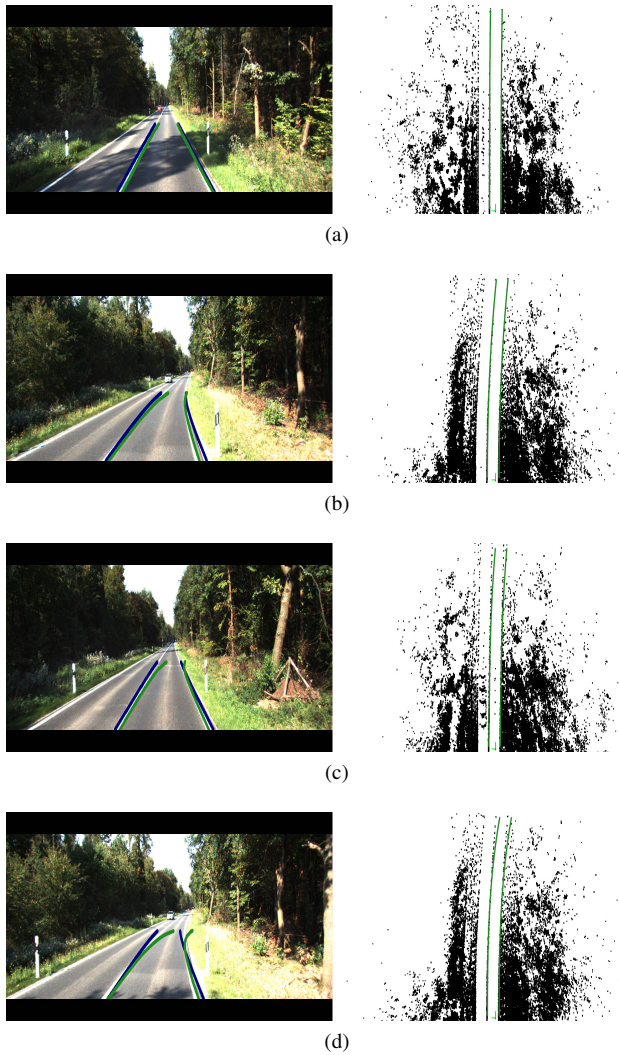


Fig. 8: Some examples of detections using the lidar, the results were projected into the image for a visual comparison with a camera solution. (a) shows a case where the lidar and camera solution correctly detects the ego lane, (b) shows a case where the camera fails due to high brightness, (c) the lidar fails where the camera does not, in (d) both of the solution fail. The color code used is as follows: green for the mean value of the ego-lane marking using lidar and blue for camera. An additional video is provided in shorturl.at/bktvE

through the program Regional competitiveness and employment 2014- 2020 (FEDER - AURA region) and by the AURA region.

REFERENCES

- [1] G. P. Team, "Global positioning system (gps) standard positioning service (sps) performance analysis report," 2014.
- [2] A. B. Hillel, R. Lerner, D. Levi, and G. Raz, "Recent progress in road and lane detection: a survey," *Machine vision and applications*, vol. 25, no. 3, pp. 727–745, 2014.
- [3] A. Hata and D. Wolf, "Road marking detection using LIDAR reflective intensity data and its application to vehicle localization," *2014 17th IEEE International Conference on Intelligent Transportation Systems, ITSC 2014*, pp. 584–589, 2014.

- [4] W. Zhang, "Lidar-based road and road-edge detection," in *2010 IEEE Intelligent Vehicles Symposium*. IEEE, 2010, pp. 845–848.
- [5] A. Hata and D. Wolf, "Road marking detection using lidar reflective intensity data and its application to vehicle localization," in *17th International IEEE Conference on Intelligent Transportation Systems (ITSC)*. IEEE, 2014, pp. 584–589.
- [6] J. Kim and M. Lee, "Robust lane detection based on convolutional neural network and random sample consensus," in *International conference on neural information processing*. Springer, 2014, pp. 454–461.
- [7] B. He, R. Ai, Y. Yan, and X. Lang, "Lane marking detection based on convolution neural network from point clouds," in *2016 IEEE 19th International Conference on Intelligent Transportation Systems (ITSC)*. IEEE, 2016, pp. 2475–2480.
- [8] L. de Paula Veronese, A. Ismail, V. Narayan, and M. Schulze, "An accurate and computational efficient system for detecting and classifying ego and sides lanes using lidar," in *2018 IEEE Intelligent Vehicles Symposium (IV)*. IEEE, 2018, pp. 1476–1483.
- [9] F. Ghallabi, F. Nashashibi, G. El-Haj-Shhade, and M.-A. Mittet, "Lidar-based lane marking detection for vehicle positioning in an hd map," in *2018 21st International Conference on Intelligent Transportation Systems (ITSC)*. IEEE, 2018, pp. 2209–2214.
- [10] A. Kasmi, D. Denis, R. Aufrere, and R. Chapuis, "Map matching and lanes number estimation with openstreetmap," in *2018 21st International Conference on Intelligent Transportation Systems (ITSC)*. IEEE, 2018, pp. 2659–2664.
- [11] —, "Probabilistic framework for ego-lane determination," in *2019 IEEE Intelligent Vehicles Symposium (IV)*. IEEE, 2019, pp. 1746–1752.
- [12] J. M. Alvarez, A. M. Lopez, T. Gevers, and F. Lumbreras, "Combining priors, appearance, and context for road detection," *IEEE Transactions on Intelligent Transportation Systems*, vol. 15, no. 3, pp. 1168–1178, 2014.
- [13] A. Joshi and M. R. James, "Generation of accurate lane-level maps from coarse prior maps and lidar," *IEEE Intelligent Transportation Systems Magazine*, vol. 7, no. 1, pp. 19–29, 2015.
- [14] F. Ramm, J. Topf, and S. Chilton, *OpenStreetMap: using and enhancing the free map of the world*. UIT Cambridge Cambridge, 2011.
- [15] J. Xiao, L. Luo, Y. Yao, W. Zou, and R. Klette, "Lane detection based on road module and extended kalman filter," in *Pacific-Rim Symposium on Image and Video Technology*, 2017, pp. 382–395.
- [16] R. Aufrere, R. Chapuis, and F. Chausse, "A model-driven approach for real-time road recognition," *Machine Vision and Applications*, vol. 13, no. 2, pp. 95–107, 2001.
- [17] L. Delobel, R. Aufrère, C. Debain, R. Chapuis, and T. Chateau, "A real-time map refinement method using a multi-sensor localization framework," *IEEE Transactions on Intelligent Transportation Systems*, vol. 20, no. 5, pp. 1644–1658, 2018.
- [18] A. Kasmi, J. Laconte, R. Aufrere, D. Denis, and R. Chapuis, "End-to-end probabilistic ego-vehicle localization framework," *IEEE Transactions on Intelligent Vehicles*, 2020.
- [19] C. Aynaud, C. Bernay-Angeletti, R. Chapuis, R. Aufrère, C. Debain, and N. Karam, "Real-time vehicle localization by using a top-down process," in *17th International Conference on Information Fusion (FUSION)*. IEEE, 2014, pp. 1–6.
- [20] C.-É. Noël Laflamme, F. Pomerleau, and P. Giguère, "Driving datasets literature review," *arXiv preprint arXiv:1910.11968*, 2019.
- [21] A. Geiger, P. Lenz, and R. Urtasun, "Are we ready for autonomous driving? the kitti vision benchmark suite," in *2012 IEEE Conference on Computer Vision and Pattern Recognition*. IEEE, 2012, pp. 3354–3361.
- [22] R. F. Berriel, E. de Aguiar, A. F. De Souza, and T. Oliveira-Santos, "Ego-lane analysis system (elas): Dataset and algorithms," *Image and Vision Computing*, vol. 68, pp. 64–75, 2017.
- [23] K. Behrendt and R. Soussan, "Unsupervised labeled lane markers using maps," in *Proceedings of the IEEE International Conference on Computer Vision Workshops*, 2019, pp. 0–0.